BIOCHEMISTRY
including biophysical chemistry & molecular biology

Article

pubs.acs.org/biochemistry

On the Mechanism of Peptidoglycan Binding and Cleavage by the *endo*-Specific Lytic Transglycosylase MltE from *Escherichia coli*

Guntur Fibriansah,[†,⊥] Francesca I. Gliubich,[‡,⊥] and Andy-Mark W. H. Thunnissen*

Laboratory of Biophysical Chemistry, Groningen Biomolecular Sciences and Biotechnology Institute, University of Groningen, Nijenborgh 7, 9747 AG Groningen, The Netherlands.

Supporting Information

ABSTRACT: The lytic transglycosylase MltE from *Escherichia coli* is a periplasmic, outer membrane-attached enzyme that cleaves the β-1,4-glycosidic bonds between *N*-acetylmuramic acid and *N*-acetylglucosamine residues in the cell wall peptidoglycan, producing 1,6-anhydromuropeptides. Here we report three crystal structures of MltE: in a substrate-free state, in a binary complex with chitopentaose, and in a ternary complex with the glycopeptide inhibitor bulgecin A and the murodipeptide *N*-acetylglucosaminyl-*N*-acetylmuramyl-L-Ala-D-Glu. The substrate-bound structures allowed a detailed analysis of the saccharide-binding interactions in six subsites of the peptidoglycan-binding groove (subsites −4 to +2) and, combined with site-directed mutagenesis analysis, confirmed the role of Glu64 as catalytic acid/base. The structures permitted the precise modeling of a short glycan strand of eight saccharide residues, providing evidence for two additional subsites (+3 and +4) and revealing the productive conformational state of the substrate at subsites −1 and +1, where the glycosidic bond is cleaved. Full accessibility of the peptidoglycan-binding groove and preferential binding of an *N*-acetylmuramic acid residue in a $^4C_1$ chair conformation at subsite +2 explain why MltE shows only *endo*- and no *exo*-specific activity toward glycan strands. The results further indicate that catalysis of glycosidic bond cleavage by MltE proceeds via distortion toward a sofa-like conformation of the *N*-acetylmuramic acid sugar ring at subsite −1 and by anchimeric assistance of the sugar's *N*-acetyl group, as shown previously for the lytic transglycosylases Slt70 and MltB.

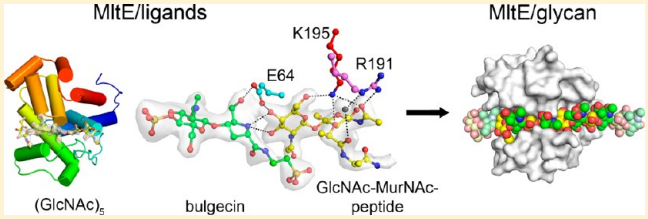

Lytic transglycosylases (LTs) are peptidoglycan degrading enzymes that function in bacterial cell wall turnover, remodeling, and maintenance.[1−3] Like lysozymes, LTs cleave the β-1,4-glycosidic bonds between the *N*-acetylmuramic acid (MurNAc) and *N*-acetylglucosamine (GlcNAc) residues of the peptidoglycan (PG) mesh (also known as murein). However, unlike lysozymes, which use hydrolysis to cleave the β-1,4-glycosidic bonds, LTs carry out an unusual intramolecular glycosyltransferase reaction, resulting in the production of nonreducing muropeptides carrying a terminal 1,6-anhydro-MurNAc residue (Scheme 1). LTs are mostly found in Gram-negative bacteria but also occur in Gram-positive bacteria as well as in a few bacteriophages. Based on the presence of conserved sequence motifs, they have been classified into four protein families, LT families 1, 2, 3, and 4.[4] The best-studied enzymes, both functionally and structurally, are those found in *Escherichia coli*. Seven different *E. coli* LTs have been described, Slt70, MltA, MltB, MltC, MltD, MltE, and MltF, with masses ranging from 26.6 to 70 kDa.[4−13] MltC, MltD, MltE, MltF, and Slt70 are members of LT family 1, while MltA and MltB are members of LT families 2 and 3, respectively.[4] All LTs of *E. coli* are located in the periplasmic space, either as a soluble protein (Slt70) or attached to the outer membrane via an N-terminal lipoyl anchor or via a single transmembrane-spanning helix. Crystal structures of Slt70 and Slt35 (a soluble fragment of MltB) revealed that the enzymes from LT families 1 and 3 possess a common catalytic domain (the LT domain) that resembles the fold of goose-type lysozyme.[5,10,14] MltA has a different β-barrel structure, which resembles the fold of endoglucanase V.[8] Most *E. coli* LTs are *exo*-enzymes that degrade PG by starting from the 1,6-anhydro-MurNAc ends of the glycan strands, thereby producing small 1,6-anhydromuropeptides containing a single GlcNAc-1,6-anhydro-MurNAc disaccharide unit. MltE, the smallest LT member, shows *endo*-specific cleavage activity and produces longer 1,6-anhydromuropeptides containing multiple disaccharide units (i.e., $(GlcNAc\text{-}MurNAc)_n$-GlcNAc-1,6-anhydro-MurNAc with n = 1, 2, or more).[7] Crystallographic binding studies of Slt70, Slt35, and MltA with PG-related compounds have identified the various amino acid residues with a role in PG binding and cleavage.[9,10,15−17] PG binding occurs in an extended groove of the enzyme composed of six saccharide subsites (numbered −4, −3, −2, −1, +1 and +2, according to Davies et al.[18]), with the terminal 1,6-anhydroMurNAc residue occupying subsite +2. Cleavage of the glycosidic bond occurs between the MurNAc and GlcNAc residue occupying subsites −1 and +1, respectively. A single catalytic residue, a glutamic acid in Slt70 and MltB or an aspartic acid in MltA, acts as a general acid/base in the catalytic mechanism of the lytic transglycosylase reaction. Catalysis most likely proceeds via formation of an oxocarbenium-like substrate

Received: July 4, 2012
Revised: October 17, 2012
Published: October 17, 2012

 © 2012 American Chemical Society

Scheme 1

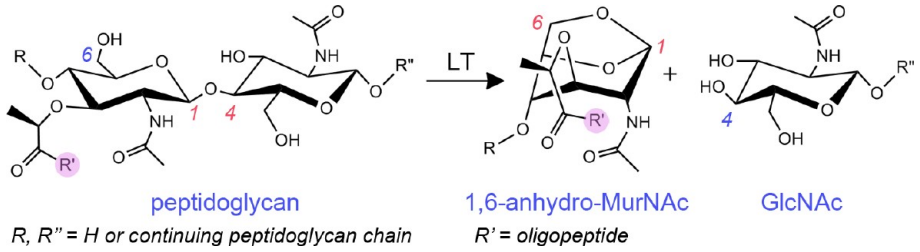

intermediate and, in the case of Slt70 and MltB, by anchimeric assistance of the sugar's *N*-acetyl group at subsite −1.[15,19,20] Steric hindrance near the +2 subsite, either by a loop or by a distinct protein domain, limits the accessibility of the groove, thus explaining the *exo*-lytic activity of Slt70, MltA, and MltB.[9,16,17]

Recently, the crystal structure of MltE was reported,[21] confirming its close structural relationship to the LT domains of Slt70 and MltB and identifying residue Glu64 as the catalytic acid/base. Like the LT domains of Slt70 and Slt35, MltE possesses an extended groove for binding PG, but the groove is fully accessible from all sides explaining the *endo*-specific activity of this enzyme. However, without structural data showing how MltE binds its substrate, the precise mechanism of PG binding and cleavage by this enzyme remains uncertain. Also, a fully accessible PG binding groove with no steric obstructions does not explain why MltE is unable to produce 1,6-anhydromuropeptides containing a single GlcNAc-1,6-anhydro-MurNAc disaccharide unit.[7] Therefore, to obtain a more complete description of its mode of action and understand its substrate binding preferences, we have determined crystal structures of *E. coli* MltE in a binary complex with chitopentaose ($(GlcNAc)_5$) and in a ternary complex with the murodipeptide GlcNAc-MurNAc-L-Ala-D-Glu and the glycopeptide bulgecin A, a specific LT inhibitor.[22] Our crystallographic results reveal the relevant saccharide binding interactions in six subsites of the PG binding groove of MltE and allow accurate modeling of the mechanism of PG binding and cleavage. In addition, the crystallographic data provide a structural basis that more accurately explains the *endo*-specific cleavage behavior of MltE.

EXPERIMENTAL PROCEDURES

Production of Soluble MltE. MltE was produced as a soluble $(His)_6$-tagged protein by overexpression in *E. coli* strain XL1-Blue carrying the plasmid pMT429-emtA.[7] The recombinant protein (named sMltE) contained 203 residues, identical to the *E. coli* MltE sequence, except that the first 16 residues, encoding the N-terminal signal peptide and lipoprotein processing site, were replaced with the sequence MRGS-$(H)_6$GSACEL. Cells were grown in standard LB medium at 30 °C and induced in log phase (A_{600} = 0.8) with 1 mM isopropyl-β-D-thiogalactopyranoside (IPTG). After 4 h of induction, cells were pelleted by centrifugation for 15 min at 10 000*g* and 4 °C, washed with washing buffer (150 mM NaCl, 50 mM Tris-HCl, pH 8.0), and resuspended in 0.5 M NaCl, 20 mM β-mercaptoethanol, 10 mM imidazole, 50 mM Tris-HCl, pH 8.0 (buffer A), supplemented with 0.2 mg/mL HEWL, 0.1% Triton, 1 mg/mL leupeptin, and 1 mg/mL pepstatin. The cells were lysed by sonication, followed by centrifugation for 30 min at 40 000*g*. The lysate was then loaded on a nickel-nitrilotriacetic acid (Ni-NTA) superflow column (Qiagen), pre-equilibrated with buffer A. After an overnight wash with 20 mM imidazole, the protein was eluted with 250 mM imidazole in buffer A. Peak fractions were pooled and dialyzed against 0.2 M NaCl, 1 mM EDTA, 1 mM DTT in 10 mM sodium phosphate buffer, pH 6.8 (buffer B), before loading onto a hydroxyapatite type I column (Bio-Rad), equilibrated in buffer B. The column was washed with buffer C (buffer B with 50 mM sodium phosphate buffer, pH 6.8), and the protein was eluted by applying a linear gradient of 50 to 400 mM phosphate buffer. Following this protocol, 8 mg of pure protein was routinely obtained per liter of culture. Selenomethionine (SeMet)-substituted sMltE was produced by standard methods using the methionine auxotrophic *E. coli* strain LE392 (Promega, Madison, WI, USA). Purification of SeMet-substituted sMltE was carried out as for the native protein, the only difference being the addition of 10 mM DTT to all solutions used. Full incorporation of seven Se atoms per protein molecule was confirmed by electrospray ionization mass spectrometry (data not shown). The purity of all protein samples was assessed by SDS-PAGE with silver staining.

Cloning and Production of sMltE-E64Q. The *mltE* gene fragment encoding for MltE residues 17−203 was amplified by PCR using plasmid pMT429-emtA as template DNA. The following primers were used: 5′-TCA CGG CGA TTA TCG CTA TCC AGT CGG GTG GTA ATC C-3′ for the forward direction and 5′-GGA TTA CCA CCC GAC TGG ATA GCG ATA ATC GCC GTG A-3′ for the reverse direction. The gene fragment was inserted into expression vector pBADnLIC using a ligation-independent cloning procedure,[23] yielding plasmid pBADnLIC-mltE. This new expression vector encoded MltE residues 17−203 with an N-terminal $(His)_{10}$-tag and a TEV (tobacco etch virus) protease cleavage site (sequence MH_{10}GENLYFQG). To allow production of the TEV-cleavable sMltE-E64Q mutant, the pBADnLIC-mltE vector was modified by site-directed mutagenesis using a Quikchange site-directed mutagenesis kit (Agilent Technologies) according to the manufacturer's instructions. Both constructs were verified by DNA sequencing. TEV-cleavable sMltE-E64Q was expressed in *E. coli* strain B834(DE3) pLysS (Novagen) carrying the modified pBADnLIC-mltE vector. The cells were grown in LB medium containing 100 μg/mL carbenicillin and 37 μg/mL chloramphenicol at 37 °C with shaking. Expression of sMltE-E64Q was induced by addition of 0.02% L-arabinose at an A_{600} of 0.8, and growth was continued for 3 h at 30 °C. Subsequent cell harvesting, lysis, and affinity-based purification using Ni-NTA chromatography were done in a similar way as for native sMltE, except for the addition of 5% glycerol to all solutions used and the presence of 40 mM imidazole in the Ni-NTA column washing buffer. Fractions containing sMltE-E64Q were pooled and dialyzed overnight against 200 mM NaCl, 1 mM EDTA, 0.5 mM DTT in 20 mM MES buffer, pH 5.0. The presence of a longer His-tag allowed sMltE-E64Q to be purified in a single step. Attempts to remove the $(His)_{10}$-tag proved unsuccessful due to aggregation of sMltE-E64Q at pH 8.0, where the TEV protease is

dx.doi.org/10.1021/bi300900t | *Biochemistry* 2012, 51, 9164−9177

Table 1. Data Collection and Refinement Statistics

	sMltE	sMltE/bulgA·GM-Ala-Glu	sMltE-E64Q/G5 (2.4 Å)	sMltE-E64Q/G5 (1.9 Å)
		Data Collection		
beamline	BW7B (DESY)	BW7B (DESY)	ID14-4 (ESRF)	BM16 (ESRF)
wavelength (Å)	0.8350	0.8420	0.9395	0.9840
space group	$P2_12_12_1$	$P2_12_12_1$	$P2_1$	$P2_1$
unit cell dimensions, *a*, *b*, *c* (Å)	77.8, 94.9, 160.5	78.8, 94.8, 162.0	71.5, 33.6, 75.2; β = 106.1°	72.0, 34.3, 77.5; β = 105.9°
max. resolution (Å)	2.25	2.3	2.4	1.9
no. of meas. reflns	352142	235955	41670	101437
No. of unique reflns	56663	54621	13461	28825
completeness (%)	98.9	98.2	97.3	98.7
R_{sym}	0.079	0.063	0.087	0.067
mean I/σ	8.2	13.1	8.5	12.1
		Refinement		
resolution range (Å)	25−2.25	23−2.3	40−2.4	40−1.9
R_{work}/R_{free} (%)[a]	18.9/22.3	16.3/20.1	24.0/28.6	21.7/26.9
composition of asymmetric unit				
protein chains	5 (aa ~20−203)	5 (aa ~19−203)	2 (aa ~21−203)	2 (aa ~21−203)
waters	420	477	73	497
ligands	3 sulfate ions	3 bulgA	1 G5, 1 G3	1 G5, 1 G4
		3 GM-Ala-Glu		2 chlorides
		3 sulfates		
average *B*-factors (Å^2)				
protein	27.0	39.0	44.3	16.5
waters	31.5	41.0	44.9	26.9
ligands	48.2	46.8	54.4	27.2
geometry				
rmsd bonds (Å)	0.010	0.009	0.010	0.011
angles (deg)	1.2	1.2	1.3	1.30
Ramachandran				
favored (%)	99.3	99.1	97.8	99.5
outliers (%)	0.0	0.0	0.0	0.0
Molprobity score	1.60	1.35	1.76	1.98
PDB entry	3T36	3T4I	3T1Z	3T21

[a] $R_{work} = \sum_{hkl}||F_{obs}|| - |F_{calc}||/\sum_{hkl}|F_{obs}|$, where the crystallographic *R*-factor was calculated with 90% of the data used in the refinement; R_{free}, the crystallographic *R*-factor based on 10% of the data withheld from the refinement for cross validation.

active. For functional assays, also TEV-cleavable native sMltE was expressed and purified, following an identical protocol as used for TEV-cleavable sMltE-E64Q.

Lytic Activity Assay. A turbidimetric assay with *Micrococcus luteus* cell wall (Sigma-Aldrich) as substrate [24] was carried out to assess the lytic activity of the sMltE proteins (native and E64Q mutant, both containing the TEV-cleavable His-tag). Insoluble *M. luteus* peptidoglycan was suspended in protein sample buffer (50 mM MES, pH 6.0, 200 mM NaCl) at a final concentration of 0.35 mg/mL. Aliquots (900 mL) of substrate suspension were mixed with 100 mL of 0.5 mg/mL sMltE. Peptidoglycan solubilization was followed by monitoring the turbidity decrease of the reaction mixture at OD_{600} for the duration of 4 h after mixing. The turbidity decrease is presented as the average of triplicate experiments and as the percentage of the initial value (extrapolated OD_{600} at t = 0 min) for the respective reaction mixture. As a control, a similar assay was performed in the absence of enzyme (only buffer).

Chitinolytic Activity Assay. The chitinolytic activity of sMltE (containing the TEV-cleavable His-tag) was assayed by determining the presence of reaction products derived from the substrate chitohexaose using thin layer chromatography (TLC). Twenty-five milliliters of a ~10 mg/mL chitohexaose (Sigma-Aldrich) solution in buffer (20 mM MES, pH 6.0, 200 mM NaCl) was mixed with enzyme (final concentration 1 mg/mL). Hen egg-white lysozyme (Sigma-Aldrich) with the same concentration was used as a control in this experiment. The reaction mixtures were incubated overnight (~20 h) at 37 °C followed by boiling for 5 min. The precipitated protein was removed by filtering through a 0.22 μm filter (Ultrafree-MC Durapore PVDF, Millipore), and the flow-through was applied to silica gel-60 F_{254} TLC plates (Merck). Chromatography was carried out using the solvent mixture *n*-propanol/25% ammonia (2:1) as eluent. The spots were stained by spraying with 10% sulfuric acid in ethanol, followed by heating at 120 °C for 30 min. Chitobiose and chitotetraose (Sigma-Aldrich) were used as standards, each at 10 mg/mL concentration. Optimum TLC results were achieved with 1.5 μL of chitobiose/chitotetraose, 2 μL of chitohexaose, 2.5 μL of sMltE/chitohexaose, and 5 μL of lysozyme/chitohexaose applied to the TLC plate.

Structure Determination of Ligand-Free sMltE. Crystals of native and SeMet-sMltE were grown by the hanging-drop vapor diffusion technique using a protein solution of ~8 mg/mL protein in sample buffer (20 mM HEPES buffer, 0.5 M NaCl, 1 mM DTT, and 1 mM EDTA, with a final of pH 5.5) and a crystallization solution of 0.1 M lithium sulfate, 15% PEG 8000 in 20 mM HEPES buffer, pH 7.5. Drops were composed of 1 μL of protein solution and 1 μL of crystallization solution. Crystals (average size ~0.3 × 0.1 × 0.05 mm^3) appeared in a few days and grew to maximum size after 3 weeks. For data collection, they

dx.doi.org/10.1021/bi300900t | *Biochemistry* 2012, 51, 9164−9177

were frozen in mother liquor complemented with 30% glycerol as cryo-protectant. Native diffraction data to 2.25 Å resolution were collected from a cryo-cooled sMltE crystal at the EMBL/DESY BW7B beamline, Hamburg. Se-MAD diffraction data were collected from a single SeMet-sMltE crystal at the ESRF BM14 beamline, Grenoble (see Table 1 and Supplementary Table S1, Supporting Information, for relevant X-ray data collection statistics). The diffraction data were indexed, integrated, and merged using the HKL software package[25] and further processed using the CCP4 software package.[26] The program Shake and Bake[27] was used to identify the positions for 24 selenium atoms using the anomalous differences in the MAD "peak" data set. MAD phases were calculated and refined with the program SHARP[28] using these positions along with the MAD diffraction data. From the residual Fourier maps, six more selenium sites were located and added to the total number of heavy atom positions for a further cycle of phase refinement. The positions of the 30 selenium sites were consistent with the presence of five sMltE molecules in the asymmetric unit. The missing selenium atoms belonged to the N-terminal selenomethionine residues in the different protein molecules, whose positions could not be determined because of disorder of the His_6-tagged termini. The final figure-of-merit was 0.53 for 2937 centric reflections and 0.57 for 26279 acentric reflections for data between 25 and 2.75 Å resolution. Phases were improved by solvent flipping, using the program SOLOMON,[29] assuming a 55% solvent content. The resulting phases were combined with the native diffraction data, extended to 2.25 Å, and further improved by multiple free-atom-model refinement using the program ARP-wARP.[30] The output model was refined in CNS[31] against the 2.25 Å diffraction data. The program QUANTA (Accelrys) was used for model rebuilding and placement of water molecules.

Structure Determination of Sugar and Muropeptide-Bound MltE Complexes. Crystals of the sMltE/bulgA·GM-Ala-Glu complex were obtained by soaking native crystals for 1 h at room temperature in a solution of 0.1 M lithium sulfate, 15% PEG 8000 in 20 mM HEPES buffer, pH 7.5, containing 10 mM bulgecin A, and 15 mM *N*-acetylglucosaminyl-*N*-acetylmuramyl-L-alanyl-D-glutamic acid (Sigma-Aldrich). The bulgecin/muropeptide-soaked crystals were transferred to a soaking solution supplemented with 30% glycerol and directly flash-frozen in liquid nitrogen. Diffraction data were collected at the BW7B beamline of the EMBL outstation at DESY, Hamburg, Germany. Data processing, model building, and refinement followed a similar procedure as for native sMltE. Crystals of the sMltE-E64Q/G5 complex were prepared by cocrystallization using the hanging-drop vapor diffusion technique. Protein drops containing chitopentaose (Sigma-Aldrich) were equilibrated at room temperature against 500 μL of reservoir solution of 0.2 M succinic acid, pH 5.5, 15% (w/v) PEG3350. It was essential to prepare the protein drops in the following order without further mixing: 1 μL of protein solution (11 mg/mL, 200 mM NaCl, 1 mM EDTA, 0.5 mM DTT, 20 mM MES pH 5.0), 2 μL of reservoir solution, and 1 μL of chitopentaose solution (2.5 mM in protein sample buffer, to achieve a 5-fold molar excess with respect to the protein). Single elongated plate-like crystals appeared within 2 days and grew to a maximum average size of ~0.3 × 0.05 × 0.02 mm^3 in a week. Crystals were soaked in paratone-N/paraffin (ratio 3:1) for cryo-protection and directly flash-frozen in liquid nitrogen. Two X-ray diffraction data sets, to 1.9 and 2.4 Å resolution, were collected at the ESRF BM16 and ID14-4 beamlines, respectively. The data sets were indexed and integrated using XDS[32] and scaled using SCALA of the CCP4 program suite[26] (Table 1). Diffraction data analysis reveals a significant Patterson peak at 0, 0, 0.5 (height ~30), indicating the presence of pseudotranslational symmetry. Structure determination was carried out by molecular replacement with the program MOLREP[33] using the apo-sMltE structure as a search model. The output model was refined against the 1.9 Å data using the program REFMAC5[34] and rebuilt in COOT.[35] At this stage in the refinement, an $F_o - F_c$ difference Fourier map, calculated with the 1.9 Å data, clearly revealed three covalently linked GlcNAc residues bound to each of the two MltE molecules in the asymmetric unit. The density was of sufficient quality to fit a chitotriose molecule to each MltE molecule, occupying subsites −3 to −1. Further refinement of the model improved the electron density maps, revealing weak electron density for two additional GlcNAc residues in subsite −4 and +1 of one protein molecule and for one additional GlcNAc residue in subsite −4 of the other protein molecule. In contrast, Fourier maps generated after refinement of the molecular replacement structure against the 2.4 Å data revealed clear electron density for a complete chitopentaose in one protein molecule and for a chitotriose in the other. COOT was used to manually build the oligosaccharides into the structures, as well as for the placement of water molecules. Final refinement cycles were carried out by using Phenix.refine[36] applying NCS restraints on the equivalent protein chains. Translation/Libration/Screw (TLS) refinement[37] was used during the final stages of the refinement. The quality of the refined structures was examined with the program Molprobity.[38] The *R*-factors (Table 1) are higher than those expected for structures solved at similar resolutions but are acceptable considering the pseudotranslational symmetry.

Structure Analysis and Modeling. Additional structure analysis was carried out using the following computer programs: T-Coffee server,[39] for multiple structure-based sequence alignment; Superpose,[40] for superimposition and calculation of root-mean-square deviations (rmsd's); and Pymol,[41] for generating figures. Construction and refinement of the glycan-bound sMltE models was performed with Coot, PyMol, and CNS. The $(GlcNAc\text{-}MurNAc)_4$-bound sMltE model was obtained by employing molecular dynamics using positional restraints to force the GlcNAc-MurNAc-GlcNAc residues in subsites −4, −3, and −2 and the GlcNAc-MurNAc residues in subsites +1 and +2 to adopt identical binding modes as the sugar residues in the sMltE-E64Q/G5 and sMltE/bulgA·GM-Ala-Glu structures, respectively. Geometric restraints were used to maintain a low energy conformation of the glycosidic linkages and sugar rings in these subsites. Based on the observed binding mode of bulgecin A in sMltE and in Slt70,[15] the MurNAc residue in subsite −1 was maintained in a sofa form with its *N*-acetyl group adopting a conformation favorable for hydrogen bonding interactions with the side chains of Gln188 and Ser73. It is important to emphasize that the positional and geometrical restraints used for the sugars were derived from the crystal structures and were necessary to guide the molecular modeling toward a high-energy productive substrate binding mode. In the absence of these restraints modeling resulted in physiologically irrelevant nonproductive binding modes.

Coordinates. The coordinates and structure factors have been deposited at the Protein Data Bank with accession codes 3T36 (apo-sMltE), 3T21 and 3T1Z (1.9 Å and 2.4 Å sMltE-E64Q/G5), and 3T4I (sMltE/bulgA·GM-Ala-Glu).

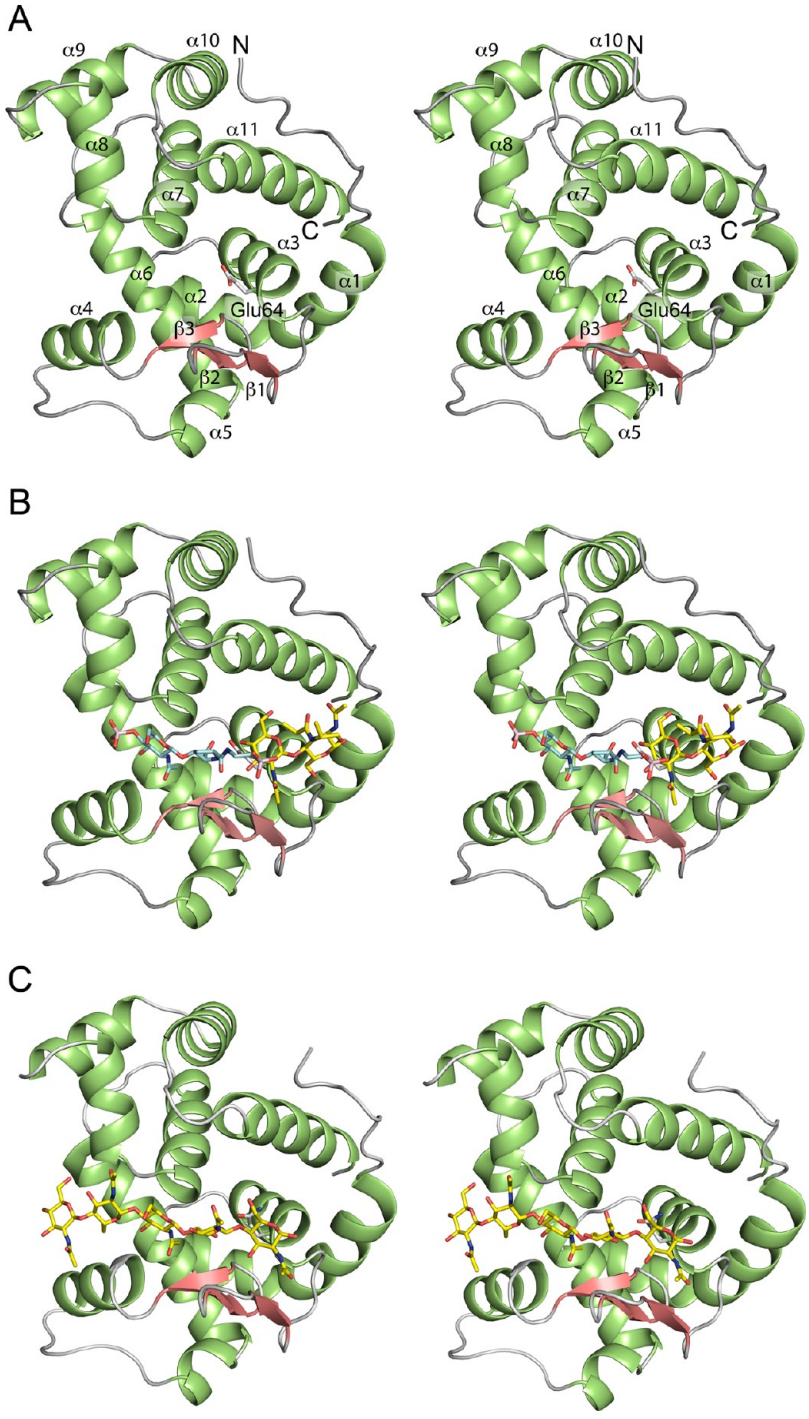

Figure 1. Ribbon stereo diagrams showing the overall structures of MltE. (A) apo-sMltE, (B) sMltE/bulgA·GM-Ala-Glu, and (C) sMltE-E64Q/G5. The bound bulgecin A, murodipeptide, and chitopentaose are shown in stick representation and labeled, with their carbon atoms colored in cyan, pink, and yellow, respectively. Other atoms are colored as follows: nitrogen, blue; oxygen, red; sulfur, orange. For apo-sMltE, the secondary structure elements are labeled, and the catalytic residue Glu64 is shown in stick representation.

RESULTS

Soluble MltE Cleaves *Micrococcus luteus* PG. A soluble, recombinant form of *E. coli* MltE (hereafter named sMltE, 203 residues), with an N-terminal polyhistidine tag replacing its lipoprotein signal sequence, was expressed and purified. Previous studies showed that sMltE is not able to cleave intact *E. coli* murein sacculi but requires removal of the peptides from the glycan strands to become optimally active.[7] Remarkably, using zymogram analysis the same studies also showed that denatured−renatured sMltE can accept murein sacculi from *Micrococcus luteus* as a substrate, which differ from the *E. coli* murein sacculi in the chemical composition of the peptide cross-bridges. To establish whether sMltE is also active against *M. luteus* murein sacculi without being first denatured and then renatured, we employed a standard turbidimetric assay (Supplementary Figure S1, Supporting Information). The results clearly confirm the lytic activity of sMltE against *M. luteus* PG. Moreover, replacement of Glu64 by a glutamine residue, using

dx.doi.org/10.1021/bi300900t | *Biochemistry* 2012, 51, 9164−9177

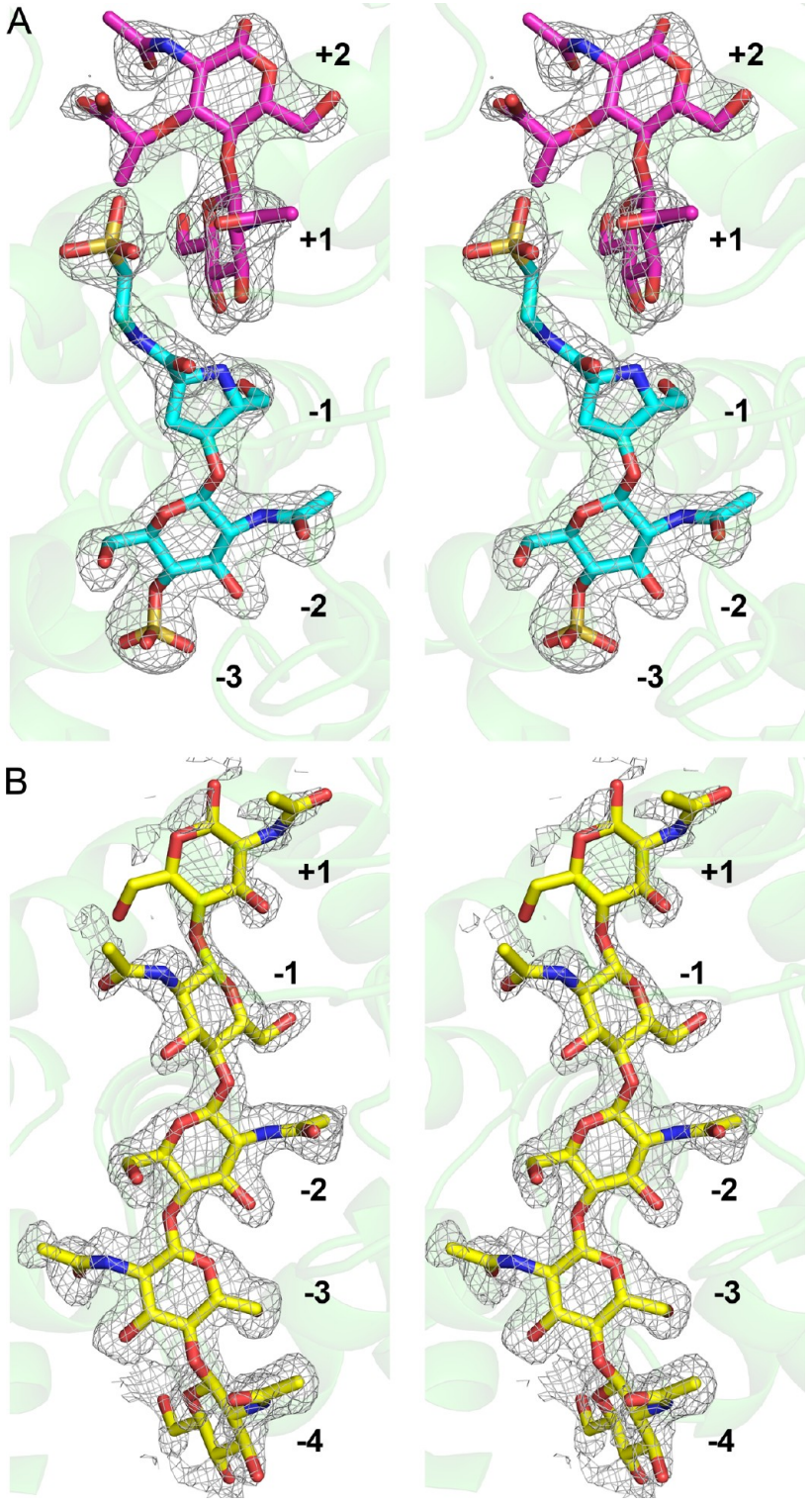

Figure 2. Stereoviews of $F_o - F_c$ simulated annealing (SA) omit maps for the ligands bound to sMltE: (A) 2.25 Å resolution SA omit map for bound bulgecin A (carbon atoms in cyan) and murodipeptide (carbon atoms in purple). The active site belongs to protein molecule A in the asymmetric unit of sMltE/bulgA·GM-Ala-Glu; (B) 1.9 Å resolution SA omit map for bound chitopentaose (carbon atoms in yellow) at the active site of molecule A in the asymmetric unit of sMltE-E64Q/G5. The maps were contoured at 2σ. Numbers indicate the different subsites.

site-directed mutagenesis, resulted in a complete abolishment of lytic activity, thus confirming the essential role of Glu64 in catalysis.

Structure Determination and Overall Structure of sMltE. Initially, the crystal structure of sMltE, in the absence of substrates or inhibitors, was solved using multiple wavelength anomalous diffraction (MAD) phases derived from selenomethionine-labeled protein and refined at 2.25 Å resolution (see Table 1 and Supporting Information for the relevant crystallographic statistics). The protein crystallized in space group $P2_12_12_1$ with five protein molecules per asymmetric unit. Noncrystallographic symmetry leads to the presence of two

dx.doi.org/10.1021/bi300900t | *Biochemistry* 2012, 51, 9164−9177

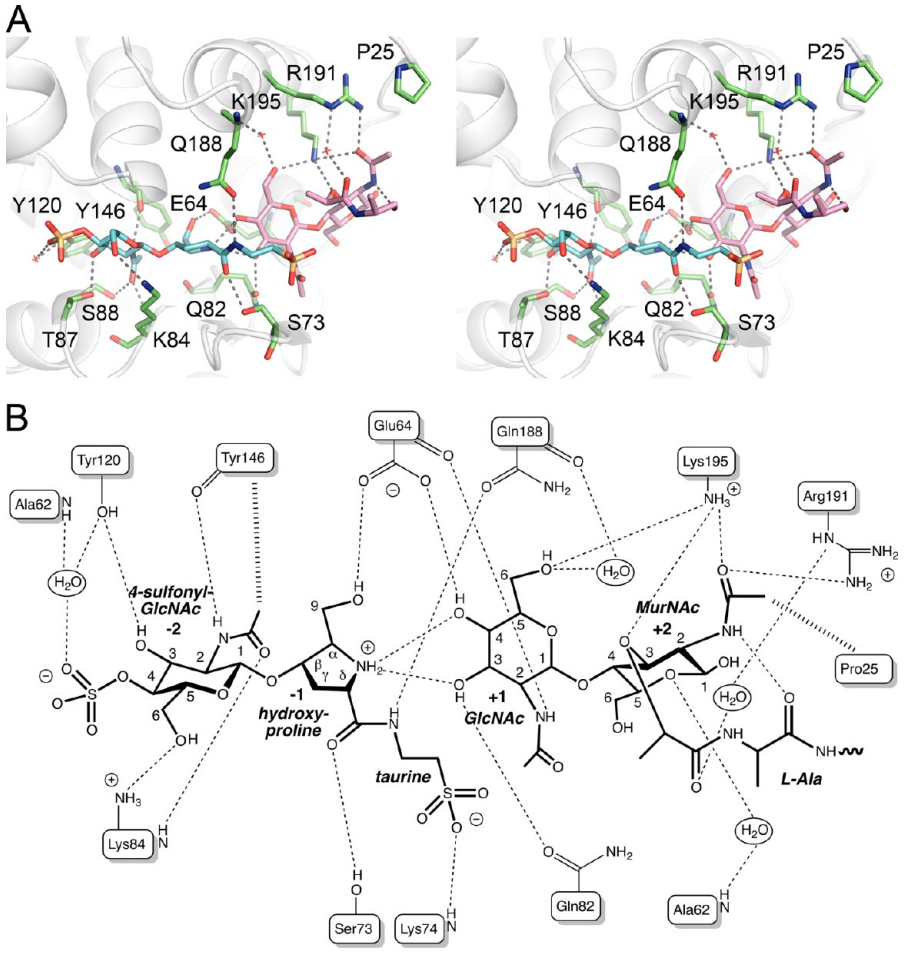

Figure 3. Interactions of sMltE with bulgecin and murodipeptide. (A) Stereoview of the substrate−protein interactions at sugar binding sites −2, −1, +1, and +2. The polypeptide chain is drawn as a light-gray ribbon, while the residues participating in substrate binding are shown as sticks, with the carbon atoms colored in green. Bulgecin A and the GlcNAc-MurNAc-L-Ala-D-Glu murodipeptide are shown as sticks with an atom coloring scheme as in Figure 1. Hydrogen bonds are shown as dashed lines. (B) Schematic drawing showing the hydrogen bond interactions (dashed lines) of bulgecin and the murodipeptide with protein residues in the active site groove. van der Waals contacts of the *N*-acetyl groups of the sugar residues with protein residues are also indicated (with different dashed lines).

distinct dimers, but we believe these dimeric configurations not to be physiologically relevant. In solution, sMltE behaves as a monomer, as judged from size exclusion chromatography and dynamic light scattering (not shown). The sMltE polypeptide chains in the asymmetric unit are well-defined by the electron density, except at the N-termini where the first 18 to 21 residues (which include the polyhistidine tag) could not be built due to disorder. The backbones of the five protein molecules are similar with pairwise root-mean-square deviations (rmsd's) in Cα positions ranging from 0.23 to 0.59 Å (for 184 residues). Significant deviations in protein conformation are only observed in loop regions on the protein surface and near the N-termini.

The overall structure of sMltE shows the typical features of the LT domain fold (Figure 1A) and is identical to the structure of *E. coli* MltE recently published by Artola-Recolons et al.[20] (rmsd in Cα positions is 0.4 ± 0.1 Å for 184 residues). Briefly, the mainly α-helical protein has a bilobal shape with a deep groove running across the surface. The N-terminal lobe contains five helices (α1−α5) and a stretch of about 20 residues inserted between helices α3 and α4 that forms a very irregular sheet of three short antiparallel β-strands (β1−β3). The C-terminal lobe is all α-helical containing five helices (α7−α11). Helix α6 in the middle of the protein is connecting the two lobes. The conserved sequence motifs characteristic of family 1 LTs are located near the center of the groove. Residue Glu64, the predicted catalytic acid/base residue of MltE, is positioned at the C-terminus of helix α3.

The sMltE Cα backbone can be superimposed on the Cα backbones of the Slt70 and Slt35 LT domains with rmsd's of 1.4 Å (116 Cα−Cα pairs, 17% sequence identity) and 1.9 Å (97 Cα−Cα pairs, 15% sequence identity), respectively. The common core of sMltE (with equivalent residues in each of the two other LTs) comprises α2, α3, β1, β2, β3, α6, and α7, while unique segments in sMltE with no equivalents in the other two proteins only include the N-terminal tail, the α4−α5 loop, and helix α9 (Supplementary Figure S2, Supporting Information). Based on its similarity to the Slt70 and Slt35 LT domains, the central groove is expected to serve as an extended PG binding site and contains at least six subsites (subsites −4 to +2). Different from the situation in the LT domains of Slt70 and Slt35, the PG binding groove in sMltE seems fully accessible for substrate over its entire length, in accordance with its endo-specific PG-cleavage activity (Supplementary Figure S3, Supporting Information).

Structures of sMltE with Peptidoglycan-Related Compounds. A 2.3 Å structure of a ternary complex of sMltE with the O-sulfonated glycopeptide bulgecin A and the murodipep-

dx.doi.org/10.1021/bi300900t | *Biochemistry* 2012, 51, 9164−9177

tide GlcNAc-MurNAc-L-Ala-D-Glu (named sMltE/bulgA·GM-Ala-Glu) was obtained by crystal soaking (Table 1, Figure 1B). Binding of the bulgecin and murodipeptide compounds was observed in only three of the five sMltE molecules that occupy the asymmetric unit; in the other two protein molecules access to the PG binding groove was blocked by crystal contacts. The two compounds bind simultaneously at nonoverlapping sites in the PG binding groove of sMltE with bulgecin A occupying subsites −2 and −1, and the murodipeptide occupying subsites +1 and +2. Electron density for the compounds is well-defined, except for the D-Glu residue of the dipeptide moiety, which appears to be disordered (Figure 2A).

In addition, a 1.9 Å structure of a binary complex of the inactive sMltE-E64Q mutant with chitopentaose (named sMltE-E64Q/G5) was obtained by cocrystallization (Table 1, Figure 1C). The crystal form of sMltE-E64Q/G5 is different than that of apo and bulgecin/murodipeptide-bound sMltE (space group $P2_1$ with two molecules per asymmetric unit). Electron density maps revealed the presence of a bound chitopentaose in subsites −4 to +1 in one of the two protein molecules (chain A) of the asymmetric unit (Figure 2B). Weaker electron density in subsites −4 and +1 points to some disorder in the binding of the terminal GlcNAc residues. However, in another crystal structure of sMltE-E64Q/G5, obtained with 2.4 Å resolution diffraction data from another crystal, the terminal GlcNAc residues of the bound chitopentaose show somewhat better defined electron density (Supplementary Figure S4, Supporting Information). In the other protein molecule (chain B), there is only density visible for four GlcNAc residues occupying subsites −4 to −1. A crystal contact with a neighboring protein molecule appears to sterically block subsite +1 in molecule B, explaining why this subsite is not occupied. Most probably, chitopentaose binds at different positions in the peptidoglycan-binding groove of sMltE with its reducing GlcNAc residue occupying either subsite −1 or +1. Enzymatic cleavage of chitopentaose to chitotetraose can be excluded, because sMltE has no chitinolytic activity (Supplementary Figure S1, Supporting Information). No significant differences in overall conformation are observed between the ligand-bound and apo-MltE structures (average rmsd in Cα backbones is 0.4 ± 0.1 Å). A small conformational difference is observed for the β-turn connecting strands β1 and β2, which has moved toward the ligands by 1−2 Å (Supplementary Figure S5, Supporting Information). Additional local conformational differences are confined to a few surface loops and the N-terminus, regions in the polypeptide not associated with substrate binding and whose conformations are probably affected by crystal packing interactions.

Binding of Bulgecin A and Murodipeptide. Binding of the two sugar−peptide compounds in sMltE/bulgA·GM-Ala-Glu is established via an extensive network of hydrogen bonds and van der Waals interactions with side chain and main chain atoms of sMltE residues that line the −2 to +2 subsites (Figure 3). Bulgecin A is bound in an extended conformation with its central GlcNAc and L-proline residues occupying subsites −2 and −1, respectively, while the proline-linked taurine group points away from subsite −1 toward the solvent. The GlcNAc-linked 4-O-sulfonate group of the bulgecin inhibitor is located in subsite −3 but has no direct interactions with the protein. The murodipeptide binds with its GlcNAc and MurNAc residues in subsites +1 and +2, respectively. All the saccharide residues of the two compounds adopt a low-energy $^4C_1$ chair conformation. Most of the interactions with the GlcNAc residues at subsites −2 and +1 and with the L-proline derivative at subsite −1 are identical to the substrate binding interactions observed previously in binary structures of Slt70 and Slt35 complexed with bulgecin A or murodipeptide (Supplementary Figure S2, Supporting Information),[14,15] further confirming the close relationships between these enzymes. Noteworthy are the interactions with the *N*-acetyl groups of the −2 and +1 GlcNAc residues, which involve three structurally highly conserved segments of family 1 LTs, including the C-terminus of the active site helix that contains the catalytic acid/base residue. As noted previously, the binding mode of the saccharide residues at the −2 and +1 subsites, with their *N*-acetyl groups buried in the back of the groove, explains why these subsites exclusively bind the alternating GlcNAc residues in a PG glycan strand: MurNAc residues are excluded at these subsites because of steric hindrance of the O3-linked peptide moieties. Also noteworthy are the interactions of the side chain carboxylate of Glu64, which forms hydrogen bonds with the α-hydroxymethyl group of the L-proline residue of bulgecin at subsite −1 and with the O4-hydroxyl group of the murodipeptide GlcNAc residue at subsite +1. Extra stabilization of the bound bulgecin inhibitor is provided by an electrostatic interaction between the positively charged, doubly protonated amine nitrogen of the L-proline ring (standard pK_a of proline's NH_2^+ is ∼10) and the negatively charged carboxylate group of Glu64 (Figure 3A). In addition, the amine nitrogen of the L-proline ring forms two hydrogen bonds with the O4 and O3 hydroxyl groups of the +1 GlcNAc residue. The amide group in the taurine moiety of bulgecin forms hydrogen bonds with Ser73 and Gln188 of sMltE, which are equivalent to the interactions of bulgecin in the active site of Slt70 with residues Ser487 and Glu583.[14] The observed binding modes of the bulgecin L-proline residue at subsite −1 and the murodipeptide GlcNAc residue at subsite +1 signify the importance of sMltE/bulgA·GM-Ala-Glu as a transition state mimic of the β-1,4-glycocidic bond cleavage reaction, as shown previously for the structures of similar complexes of Slt70 and Slt35.[15,17] In addition, the observed hydrogen bond interactions of bulgecin with Ser73 and Gln188 are indicative of a substrate-assisted reaction mechanism, with participation of the *N*-acetyl group of −1 MurNAc residue stabilizing the oxocarbenium intermediate, as previously proposed for Slt70.[15]

While subsites −2, −1, and +1 of sMltE are structurally and functionally highly similar to the equivalent subsites in the other LTs, subsite +2 of sMltE shows significant differences. In the structure of Slt70 with the murotripeptide GlcNAc-1,6-anhydroMurNAc-L-Ala-D-Glu-mDAP (GanhM-Ala-Glu-Dap), subsite +2 is occupied by a terminal 1,6-anhydroMurNAc residue, but binding of this residue is mostly stabilized via specific interactions with the oligopeptide moiety that is linked to the lactyl group of the sugar.[16] Similarly, binding of the MurNAc residue at subsite +2 in the structure of Slt35/GM-Ala-Glu mainly occurs via interactions with the oligopeptide moiety of the sugar residue.[15] In contrast, in the sMltE/bulgA·GM-Ala-Glu complex, the MurNAc residue bound at subsite +2 forms several hydrogen bonds with the enzyme, while there are no interactions with the peptide moiety, which remains largely disordered. Residue Lys195 of helix α11 plays a prominent role in binding the murodipeptide: its side chain forms hydrogen bonds with the *N*-acetyl oxygen atom and O3 hydroxyl of the +2 MurNAc residue, as well as with the O6 hydroxyl of the +1 GlcNAc residue. Another important saccharide-binding residue at subsite +2 is Arg191 of helix α11, which forms a direct hydrogen bond with the *N*-acetyl oxygen atom and a water-meditated hydrogen bond with the lactyl group of the MurNAc residue. The residues

dx.doi.org/10.1021/bi300900t | *Biochemistry* 2012, 51, 9164−9177

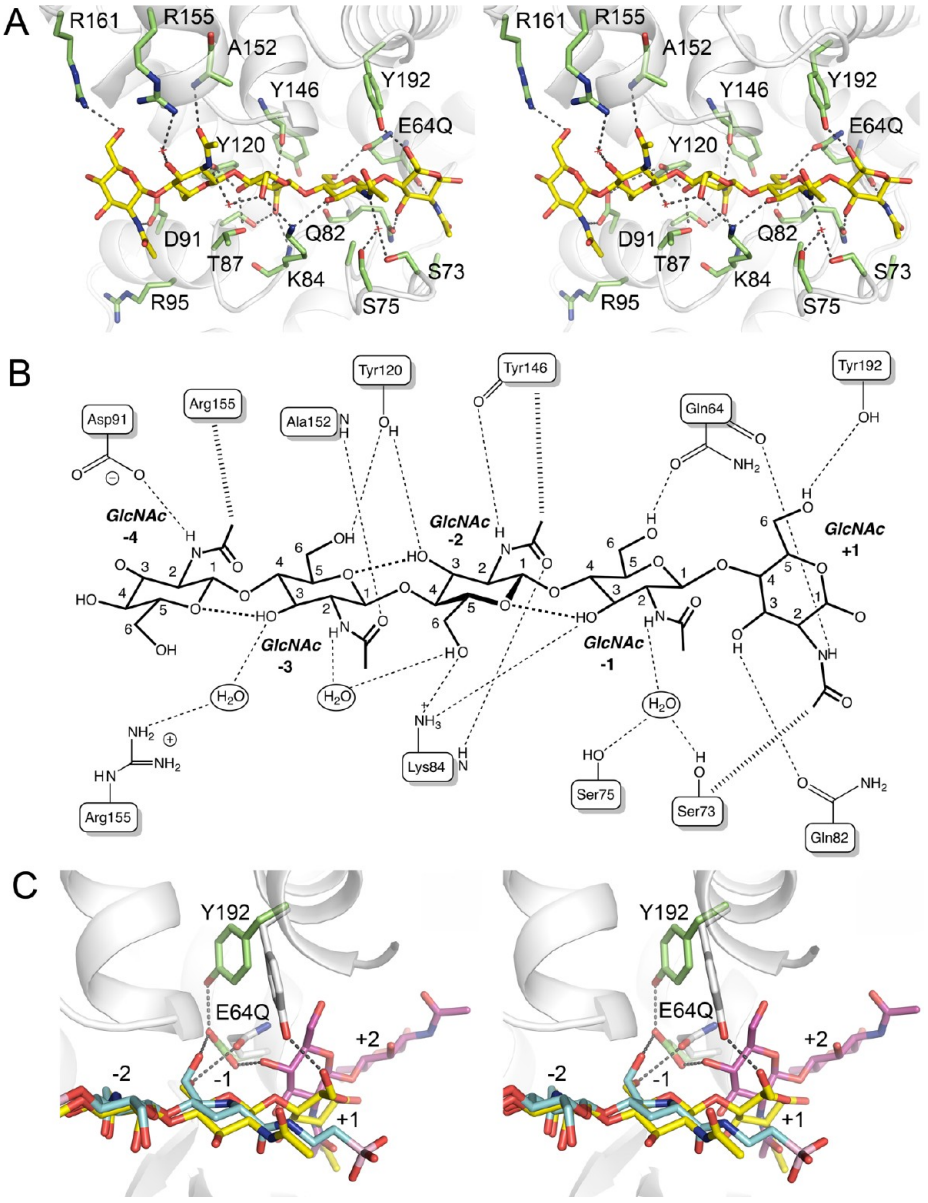

Figure 4. Interactions of sMltE-E64Q with chitopentaose. (A) Stereoview of the sugar−protein interactions at the five sugar binding sites −4, −3, −2, −1, and +1. Presentation and coloring scheme as in Figure 1. Hydrogen bonds are shown as dashed lines. (B) Schematic drawing showing the hydrogen bond interactions (dashed lines) and van der Waals contacts (different dashed lines, *N*-acetyl groups only) of chitopentaose in the active site groove of sMltE-E64Q. (C) Stereoview showing a superposition of bound bulgecin/murodipeptide and bound chitopentaose in the active site groove of sMltE, focusing on subsites −2, −1, +1, and +2. Shown in sticks are the side chains of residues 64 and 192, revealing the conformational differences of these residues in the two structures. Colors are as in Figure 1 with protein carbon atoms of sMltE/bulgA·GM-Ala-Glu, and sMltE-E64Q/G5 colored in green and gray, respectively.

of MltE that participate in the binding of the MurNAc residue at subsite +2 are not conserved in Slt70 and MltB (Supplementary Figure S2, Supporting Information). However, they are highly conserved in the amino acid sequences of MltE orthologs, suggesting that the specific substrate binding interactions at subsite +2 are crucial for the correct functioning of this enzyme.

Binding of Chitopentaose. The interactions of the chitin-derived pentasaccharide that is bound at subsites −4 to +1 of sMltE are shown in Figure 4. All GlcNAc residues in the pentasaccharide adopt a full, low-energy $^4C_1$ chair conformation. The glycosidic bond conformations are similar to that observed in chitin, except for the glycosidic linkage between the −1 and +1 GlcNAc residues, where bond rotations resulted in a loss of the intramolecular hydrogen bond between the O3 hydroxyl of the +1 GlcNAc and the sugar ring O5 oxygen of the −1 GlcNAc residue. A structural comparison of sMltE-E64Q/G5 and sMltE/bulgA·GM-Ala-Glu (Figure 4C) reveals that the −2 GlcNAc residue of the bound chitopentaose has an identical binding mode as the −2 GlcNAc residue of bulgecin A, while the −1 GlcNAc is bound very similarly to the L-proline derivative of bulgecin A, with its 5-hydroxymethyl group at hydrogen bonding distance to the side chain of Gln64. However, the +1 GlcNAc residue of the chitopentaose is bound less deeply and with a slightly different orientation inside its subsite than the +1 GlcNAc residue of the murodipeptide in sMltE/bulgA·GM-Ala-Glu. As a consequence, the oxygen of −1 to +1 glycosidic bond in sMltE/G5 is too far away from the side chain of Gln64 to form a hydrogen bond. Despite its shifted position, the GlcNAc residue

dx.doi.org/10.1021/bi300900t | *Biochemistry* 2012, 51, 9164−9177

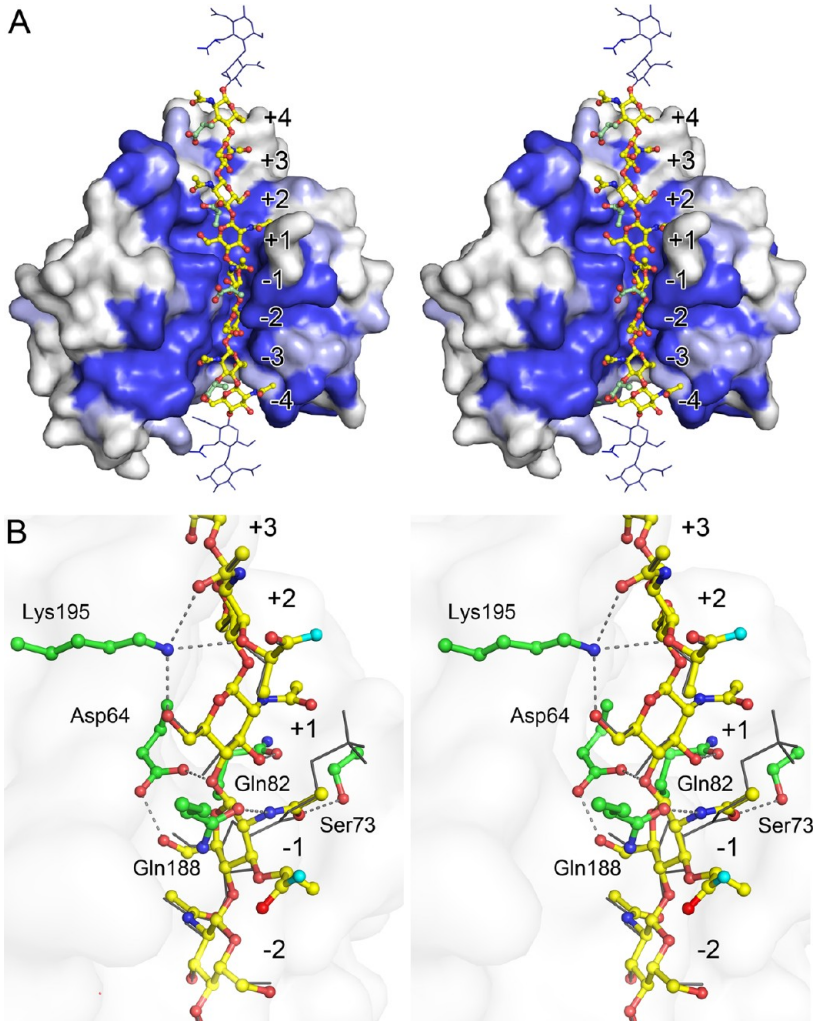

Figure 5. Glycan-bound model of sMltE. (A) View of a modeled $(GlcNAc\text{-}MurNAc)_4$ glycan fragment (sticks, yellow carbons) bound in the PG binding groove of sMltE. At each side of $(GlcNAc\text{-}MurNAc)_4$ an additional (GlcNAc-MurNAc) unit is drawn (lines, blue carbon atoms) to emphasize the full accessibility of the PG binding groove. Sugar binding subsites are labeled. The protein is shown in a molecular surface representation with residues that are highly conserved among MltEs from different bacteria highlighted in blue. (B) Close-up view showing a superposition of the $(GlcNAc\text{-}MurNAc)_4$-bound sMltE model and the sMltE/bulgA·GM-Ala-Glu structure focusing on subsites −2, −1, +1, and +2. Bulgecin and the murodipeptide are colored in light gray, while $(GlcNAc\text{-}MurNAc)_4$ is colored as in panel A (yellow carbons). Note the sofa-like conformation of the −1 MurNAc residue of $(GlcNAc\text{-}MurNAc)_4$ and the proposed interactions of its *N*-acetyl group with Ser73 and Gln188 (in green), stabilizing a conformation that allows anchimeric assistance in catalysis.[15,20]

at subsite +1 in sMltE/G5 forms similar hydrogen bonds as the +1 GlcNAc residue in sMltE/bulgA·GM-Ala-Glu. A remarkable difference, though, concerns the interaction of the 5-hydroxymethyl group of the +1 GlcNAc residue of chitopentaose, which is too far away to form a hydrogen bond with Lys195 like in sMltE/bulgA·GM-Ala-Glu. Instead, it forms a hydrogen bond with the side chain of Tyr192. In the unliganded sMltE and sMltE/bulgA·GM-Ala-Glu structures, Tyr192, which is strictly conserved among LT1 and LT3 family members, has its side chain inside a pocket behind the catalytic acid/base, forming a hydrogen bond to one of the carboxylate oxygen atoms of Glu64 (Figure 4C). However, in sMltE-E64Q/G5 the side chain of Tyr192 has swung out from its binding pocket due to a ∼75° Cα−Cβ bond rotation, disrupting the interaction with residue 64 and allowing its hydroxyl group be accessed by the +1 GlcNAc residue.

The sMltE-E64Q/G5 structure further reveals the specific saccharide binding interactions that occur in subsites −4 and −3 of the PG binding groove of MltE. Various hydrogen bonds and van derWaals interactions are formed with the −3 GlcNAc residue, but the −4 GlcNAc is less tightly bound, as is evident from the weaker electron density and higher average B-factor associated with this sugar residue compared with the sugar residue in subsite −3. In contrast to subsites −2, −1, and +1, the amino acid residues that form the sugar binding interactions at subsites −4 and −3 are not conserved in Slt70 and Slt35, which is not surprising considering the larger distance of these subsites away from the active site.

Modeling of Peptidoglycan-Bound MltE. The crystallographic binding studies allowed us to characterize the subsites in the PG-binding groove of MltE that bind bulgecin A, murodipeptide, and chitopentaose. To further reveal the relevance of the structural data for understanding PG binding and cleavage by MltE, we used the two complex structures as templates to construct a protein model of sMltE bound with $(GlcNAc\text{-}MurNAc)_4$ (Figure 5). The choice for this substrate was based on previous kinetic experiments by Kraft et al.,[7] showing that MltE prefers to cleave glycan chains that miss the

dx.doi.org/10.1021/bi300900t | *Biochemistry* 2012, 51, 9164−9177

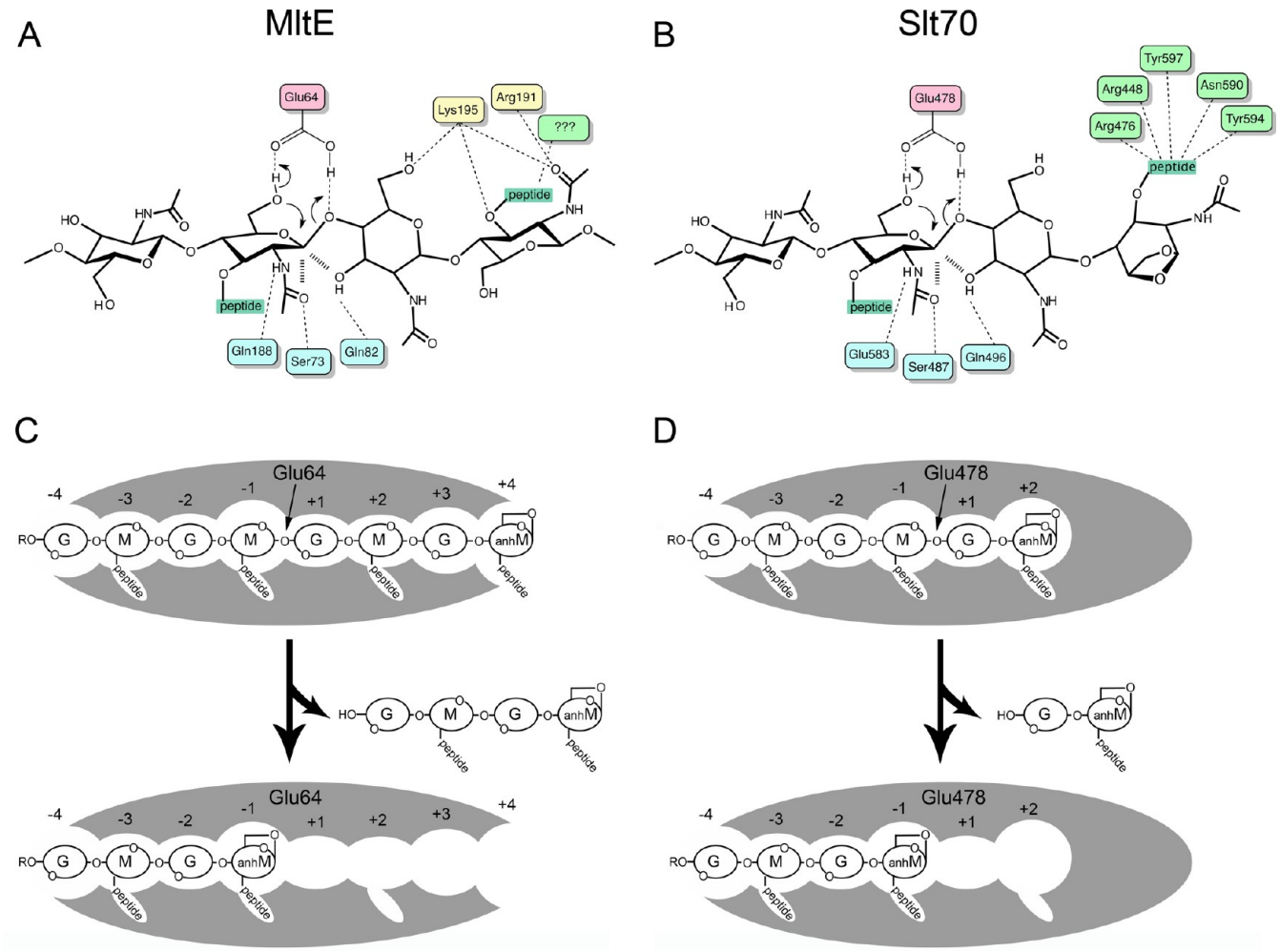

Figure 6. Proposed productive binding modes and cleavage of peptidoglycan (PG) in the PG-binding grooves of MltE and Slt70. (A, B) Binding modes of PG in subsites −2, −1, +1, and +2 of MltE and Slt70. While the interactions with the −1 MurNAc residue and the scissile glycosidic bond are highly conserved, the interactions with the muropeptide residue at subsite +2 are different. MltE specifically recognizes the saccharide moiety of the +2 muropeptide residue, whereas Slt70 recognizes the peptide moiety. (C, D) Extended binding modes of PG across the grooves of MltE and Slt70 and its resulting cleavage pattern. In MltE, the groove is accessible from both sides, explaining its *endo*-lytic activity. The loose subsite +4 accepts both a MurNAc and 1,6-anhydroMurNAc residue, but the tight subsite +2 only accepts a MurNAc residue, explaining why the 1,6-anhydro-muropeptide products contain minimally four saccharide residues. Note that when subsite +4 accepts a MurNAc residue, the cleavage product would be $(G\text{-}M)_n$-G-anhM, with $n = 2$ or more. In Slt70, the groove is blocked after subsite +2, explaining why it has *exo*-lytic activity and why its 1,6-anhydro-muropeptide products contain two saccharide residues.

peptides and that are at least four disaccharide units long. In the model, the first three GlcNAc-MurNAc disaccharide units of the glycan chain occupy subsites −4 to +2 of sMltE, while the terminal GlcNAc-MurNAc unit is located at the end of the groove, possibly identifying two additional subsites, that is, +3 and +4. No direct hydrogen bonding interactions with the sugar residues could be discerned at subsites +3 and +4, though, and the sugar residues are significantly exposed to the solvent, suggesting that the binding of a GlcNAc-MurNAc unit in these subsites is rather loose. There is no steric obstruction that would prevent the glycan chain to be extended on both ends with additional disaccharide units but such residues will completely stick into the solvent (Figure 5A). Furthermore, with the −1 MurNAc residue in a sofa conformation the glycosidic bond between the −1 and +1 sugars could be modeled in the same position as the O4 hydroxyl of the GlcNAc residue of the murodipeptide in sMltE/bulgA·GM-Ala-Glu, while the 5-hydroxymethyl group of the −1 MurNAc occupied a position equivalent to that of the α-hydroxymethyl group in bulgecin, thus allowing both the glycosidic bond oxygen and the 5-hydroxymethyl group to interact with Glu64 (Figure 5B). It is important to note that such a binding mode could not be obtained with the −1 MurNAc in a low-energy $^4C_1$ chair conformation. To allow a binding mode of the +1 and +2 saccharides like that observed for the murodipeptide in sMltE/bulgA·GM-Ala-Glu, the −1 to +1 glycosidic linkage had to be rotated away from its energetically most favorable conformation, thereby losing the intramolecular hydrogen-bonding interaction between the O3 hydroxyl group of the +1 GlcNAc and the −1 MurNAc O5 ring oxygen. Instead, the O3 hydroxyl group of the +1 GlcNAc is hydrogen bonded to the strictly conserved Gln82 and is positioned under the C1 carbon of the +1 GlcNAc at a close distance of 3 Å.

In addition to the $(GlcNAc\text{-}MurNAc)_4$ glycan fragment, modeling was performed with glycan fragments carrying a terminal 1,6-anhydroMurNAc residue. The largely exposed MurNAc residue at subsite +4 in the $(GlcNAc\text{-}MurNAc)_4$-bound sMltE model could easily be replaced by a 1,6-

dx.doi.org/10.1021/bi300900t | *Biochemistry* 2012, 51, 9164−9177

anhydroMurNAc residue, without introducing unfavorable contacts. However, at subsite +2, it was not possible to satisfactorily model a bound 1,6-anhydroMurNAc residue, without introducing several close contacts or disrupting the hydrogen bonds with Arg191 and Lys195. This suggests that subsite +2 in sMltE is specific toward binding an internal MurNAc residue and unsuitable for binding a terminal 1,6-anhydroMurNAc residue of a glycan chain.

DISCUSSION

Our analysis of the sMltE/bulgA·GM-Ala-Glu and sMltE-E64Q/G5 crystal structures provides clear experimental evidence how a murein glycan strand binds in the extended PG-binding groove of MltE. The structures identify the saccharide-binding interactions at subsites −4 to +2, while modeling suggests the existence of two additional subsites, that is, +3 and +4. In particular, our results underline the close relationships of MltE with the LT-domains of Slt70 and MltB. As expected, the structural similarities are most pronounced between MltE and the LT-domain of Slt70. The saccharide-binding interactions at subsites −2, −1, and +1 are highly conserved in these LT family 1 members, and the combined structural data revealed by the current study strongly suggests that MltE uses a similar substrate-assisted reaction mechanism as previously described for Slt70 and MltB,[15,19,20] with Glu64 acting as a general acid/base catalyst, while Ser73 and Gln188 prime the −1 MurNAc *N*-acetyl group for anchimeric assistance (Figures 5B and 6A,B).

A few important differences can be discerned when the PG-binding groove of MltE is compared with that of Slt70 and MltB, differences that contribute to the unique *endo*-specific cleavage activity of MltE. As noted previously, the groove in MltE is fully accessible from both sides and lacks any steric obstruction near the +2 subsite (Figure 6C, Supplementary Figure S3, Supporting Information). Additionally, our results show that, in contrast to Slt70 and MltB, the +2 subsite of MltE is adapted to optimally bind a MurNAc residue with its sugar ring in a low-energy $^4C_1$ chair conformation and is much less suited for binding the terminal 1,6-anhydroMurNAc residue (in a $^1C_4$ chair conformation) of a glycan chain, which would be necessary for *exo*-lytic activity (Figure 6C,D). This also explains why MltE cleaves at a distance of two or more disaccharide units from the 1,6-anhydroMurNAc end of the glycan chain and why it requires a glycan chain of at least four disaccharide units in length, that is, $(GlcNAc\text{-}MurNAc)_3$-GlcNAc-1,6-anhydroMurNAc is cleaved, but $(GlcNAc\text{-}MurNAc)_2$-GlcNAc-1,6-anhydroMurNAc is not.[5] Apparently, the minimal requirement for productive binding and cleavage of a glycan strand by MltE is that subsites −4 to +2 are occupied with three consecutive (GlcNAc-MurNAc) disaccharide units, while subsites +3 and +4 may be either occupied with another internal (GlcNAc-MurNAc) unit or a terminal GlcNAc-1,6-anhydroMurNAc disaccharide (Figure 6C). The hexasaccharide $(GlcNAc\text{-}MurNAc)_2$-GlcNAc-1,6-anhydroMurNAc may perhaps still bind to subsites −4 to +2, but is not cleaved, because with a 1,6-anhydroMurNAc residue at subsite +2 insufficient binding energy will be generated to obtain the necessary conformational distortion of the −1 MurNAc residue and the −1 to +1 glycosidic linkage in the substrate.

A surprising finding in the sMltE-E64Q/G5 crystal structure is the uncommon outward side chain conformation of the highly conserved Tyr192 residue at subsite +1. What exactly causes this conformational change of Tyr192 is unclear. The conformational change is not dependent on the presence of the terminal GlcNAc residue of the chitopentaose at subsite +1, as the outward side chain conformation of Tyr192 is also observed in protein molecule B of sMltE-E64Q/G5, in which subsite +1 is not occupied. This may indicate that the conformational change of Tyr192 is somehow caused by the mutation of Glu64 to a glutamine, but considering that in the interaction with Tyr192 the Glu64 side chain is acting as a hydrogen bond acceptor, a glutamine residue should be able to replace Glu64 without causing a change in hydrogen bonding geometry. Obviously, the observed flexibility of the Tyr192 side chain needs further investigation including a determination of the crystal structure of apo sMltE-E64Q.

It remains unclear whether MltE binds the peptide moieties that are attached to the MurNAc residues in peptidoglycan. The conserved surface residues that are found near the −3, −1, and +2 subsites of MltE (Figure 5A) could point out the location of specific peptide binding sites. Artola-Recolons et al.[21] point out potential peptide-binding sites in the unliganded structure of MltE by modeling. However, the current structural data of MltE do not allow a reliable assessment whether such peptide binding sites really exist, also considering that no experimental information is available that indicates amino acid residues in MltE with a role in peptide binding. In fact, the studies by Kraft et al. revealed that MltE, unlike Slt70, is optimally active on isolated murein glycan strands that lack the peptide moieties.[7] Considering its inability to cleave chitin (Supplementary Figure S1, Supporting Information), it thus seems that the enzyme only requires the presence of the C3-lactyl groups of the MurNAc residues for its activity, while the peptides attached to the lactyl groups in PG play no important role in substrate binding and cleavage. However, the same studies by Kraft et al. also revealed that MltE is unable to hydrolyze intact *E. coli* murein sacculi *in vitro*, while its overproduction *in vivo* does not result in rapid bacteriolysis, indicating that the peptides have a strong inhibitory effect. Our observation that MltE is able to cleave the intact cell wall of *M. luteus*, which differs from the *E. coli* cell wall in its PG peptide composition, further signifies that this inhibitory effect of the peptides is probably caused by specific binding and is not due to steric hindrance. Possibly, binding by MltE of the peptide moieties in its natural substrate forces the bound glycan chain into an unproductive conformation, rendering it resistant to cleavage. Alternatively, it may prohibit the glycan chain to be released from the binding groove of MltE after cleavage, causing the enzyme to stall. Such a substrate-specific control of the lytic activity could serve as a means to spatially and temporally regulate this potentially suicidal enzyme *in vivo*, and perhaps MltE needs to act together with a PG amidase in order to become fully functional.[7] Unfortunately, very little functional data is available on MltE, and its specific role in PG metabolism is still unclear.[42] It is evident that more functional and structural investigations are required to fully understand the physiological role and behavior of this enzyme.

ASSOCIATED CONTENT

Supporting Information

Table with relevant phasing statistics, figures of the peptidoglycanolytic and chitinolytic assays, multiple sequence alignment and structural comparison of MltE, Slt70, and MltB, $2F_o - F_c$ electron density maps of the bound ligands, and overlays of the apo and ligand-bound sMltE structures. This material is available free of charge via the Internet at http://pubs.acs.org.

AUTHOR INFORMATION

Corresponding Author

*Phone: +31 50 3634380. E-mail: a.m.w.h.thunnissen@rug.nl.

Present Addresses

[†]Laboratory of Virus Structure and Function, Duke-NUS Graduate Medical School, 8 College Road, Singapore 169857.

[‡]Office of the Vice-Principal for Health, Old Anatomy Building, Barts and the London School of Medicine and Dentistry, Queen Mary University of London, Charterhouse Square, London EC1M 6BQ.

Author Contributions

[⊥]G.F. and F.I.G. contributed equally to this work.

Funding

G.F. was supported by an Ubbo Emmius Bursary Fellowship from the University of Groningen, F.I.G. by a European Union Marie Curie Individual Fellowship and by an EMBO long term fellowship.

Notes

The authors declare no competing financial interest.

ACKNOWLEDGMENTS

The plasmid pMT429-emtA was obtained from Prof. Joachim-Volker Höltje, Tübingen. We gratefully acknowledge the ESRF, Grenoble, and EMBL/DESY, Hamburg, and their MX staff members, for provision of synchrotron radiation facilities and assistance in using the beamlines.

ABBREVIATIONS

GlcNAc, *N*-acetylglucosamine; LT, lytic transglycosylase; Mlt, membrane-bound lytic transglycosylase; MurNAc, *N*-acetylmuramic acid; PG, peptidoglycan; rmsd, root-mean-square deviation; Slt, soluble lytic transglycosylase; sMltE, soluble recombinant form of membrane-bound lytic transglycosylase E from *E. coli*

REFERENCES

(1) Höltje, J. V. (1996) Lytic transglycosylases. *EXS 75*, 425−429.

(2) Scheurwater, E., Reid, C. W., and Clarke, A. J. (2008) Lytic transglycosylases: Bacterial space-making autolysins. *Int. J. Biochem. Cell Biol. 40*, 586−591.

(3) van Heijenoort, J. (2011) Peptidoglycan hydrolases of *Escherichia coli*. *Microbiol. Mol. Biol. Rev. 75*, 636−663.

(4) Blackburn, N. T., and Clarke, A. J. (2001) Identification of four families of peptidoglycan lytic transglycosylases. *J. Mol. Evol. 52*, 78−84.

(5) Thunnissen, A. M. W. H., Dijkstra, A. J., Kalk, K. H., Rozeboom, H. J., Engel, H., Keck, W., and Dijkstra, B. W. (1994) Doughnut-shaped structure of a bacterial muramidase revealed by X-ray crystallography. *Nature 367*, 750−753.

(6) Dijkstra, A. J., and Keck, W. (1996) Identification of new members of the lytic transglycosylase family in *Haemophilus influenzae* and *Escherichia coli*. *Microb. Drug Resist. 2*, 141−145.

(7) Kraft, A. R., Templin, M. F., and Höltje, J. V. (1998) Membrane-bound lytic endotransglycosylase in *Escherichia coli*. *J. Bacteriol. 180*, 3441−3447.

(8) van Straaten, K. E., Dijkstra, B. W., Vollmer, W., and Thunnissen, A. M. W. H. (2005) Crystal structure of MltA from reveals a unique lytic transglycosylase fold. *J. Mol. Biol. 352*, 1068−1080.

(9) van Straaten, K. E., Barends, T. R., Dijkstra, B. W., and Thunnissen, A. M. W. H. (2007) Structure of *Escherichia coli* lytic transglycosylase MltA with bound chitohexaose: Implications for peptidoglycan binding and cleavage. *J. Biol. Chem. 282*, 21197−21205.

(10) van Asselt, E. J., Dijkstra, A. J., Kalk, K. H., Takacs, B., Keck, W., and Dijkstra, B. W. (1999) Crystal structure of *Escherichia coli* lytic transglycosylase Slt35 reveals a lysozyme-like catalytic domain with an EF-hand. *Structure 7*, 1167−1180.

(11) Suvorov, M., Lee, M., Hesek, D., Boggess, B., and Mobashery, S. (2008) Lytic transglycosylase MltB of *Escherichia coli* and its role in recycling of peptidoglycan strands of bacterial cell wall. *J. Am. Chem. Soc. 130*, 11878−11879.

(12) Scheurwater, E. M., and Clarke, A. J. (2008) The C-terminal domain of *Escherichia coli* YfhD functions as a lytic transglycosylase. *J. Biol. Chem. 283*, 8363−8373.

(13) Madoori, P. K., and Thunnissen, A. M. W. H. (2010) Purification, crystallization and preliminary X-ray diffraction analysis of the lytic transglycosylase MltF from *Escherichia coli*. *Acta Crystallogr. F66*, 534−538.

(14) Thunnissen, A. M. W. H., Isaacs, N. W., and Dijkstra, B. W. (1995) The catalytic domain of a bacterial lytic transglycosylase defines a novel class of lysozymes. *Proteins 22*, 245−258.

(15) Thunnissen, A. M. W. H., Rozeboom, H. J., Kalk, K. H., and Dijkstra, B. W. (1995) Structure of the 70-kDa soluble lytic transglycosylase complexed with bulgecin A: Implications for the enzymatic mechanism. *Biochemistry 34*, 12729−12737.

(16) van Asselt, E. J., Thunnissen, A. M. W. H., and Dijkstra, B. W. (1999) High resolution crystal structures of the *Escherichia coli* lytic transglycosylase Slt70 and its complex with a peptidoglycan fragment. *J. Mol. Biol. 291*, 877−898.

(17) van Asselt, E. J., Kalk, K. H., and Dijkstra, B. W. (2000) Crystallographic studies of the interactions of *Escherichia coli* lytic transglycosylase Slt35 with peptidoglycan. *Biochemistry 39*, 1924−1934.

(18) Davies, G. J., Wilson, K. S., and Henrissat, B. (1997) Nomenclature for sugar-binding subsites in glycosyl hydrolases. *Biochem. J. 321* (Pt 2), 557−559.

(19) Reid, C. W., Blackburn, N. T., Legaree, B. A., Auzanneau, F. I., and Clarke, A. J. (2004) Inhibition of membrane-bound lytic transglycosylase B by NAG-thiazoline. *FEBS Lett. 574*, 73−79.

(20) Reid, C. W., Legaree, B. A., and Clarke, A. J. (2007) Role of Ser216 in the mechanism of action of membrane-bound lytic transglycosylase B: Further evidence for substrate-assisted catalysis. *FEBS Lett. 581*, 4988−4992.

(21) Artola-Recolons, C., Carrasco-López, C., Llarrull, L. I., Kumarasiri, M., Lastochkin, E., Martinez de Ilarduya, I., Meindl, K., Usón, I., Mobashery, S., and Hermoso, J. A. (2011) High-resolution crystal structure of MltE, an outer membrane-anchored endolytic peptidoglycan lytic transglycosylase from *Escherichia coli*. *Biochemistry 50*, 2384−2386.

(22) Templin, M. F., Edwards, D. H., and Holtje, J. V. (1992) A murein hydrolase is the specific target of bulgecin in *Escherichia coli*. *J. Biol. Chem. 267*, 20039−20043.

(23) Geertsma, E. R., and Poolman, B. (2007) High-throughput cloning and expression in recalcitrant bacteria. *Nat. Methods 4*, 705−707.

(24) Hash, J. H. (1967) Measurement of bacteriolytic enzymes. *J. Bacteriol. 93*, 1201−1202.

(25) Otwinowski, Z., and Minor, W. (1997) *Methods Enzymol. 276*, 307−326.

(26) Collaborative Computational Project, Number 4 (1994) The CCP4 suite: Programs for protein crystallography. *Acta Crystallogr. D50*, 760−763.

(27) Weeks, C. M., and Miller, R. (1999) Optimizing shake-and-bake for proteins. *Acta Crystallogr. D55*, 492−500.

(28) Bricogne, G., Vonrhein, C., Flensburg, C., Schiltz, M., and Paciorek, W. (2003) Generation, representation and flow of phase information in structure determination: Recent developments in and around SHARP 2.0. *Acta Crystallogr. D59*, 2023−2030.

(29) Abrahams, J. P., and Leslie, A. G. (1996) Methods used in the structure determination of bovine mitochondrial F1 ATPase. *Acta Crystallogr. D52*, 30−42.

(30) Cohen, S. X., Ben Jelloul, M., Long, F., Vagin, A., Knipscheer, P., Lebbink, J., Sixma, T. K., Lamzin, V. S., Murshudov, G. N., and Perrakis, A. (2008) ARP/wARP and molecular replacement: The next generation. *Acta Crystallogr. D64*, 49−60.

(31) Brünger, A. T. (2007) Version 1.2 of the crystallography and NMR system. *Nat. Protoc. 2*, 2728−2733.
(32) Kabsch, W. (1993) Automatic processing of rotation diffraction data from crystals of initially unknown symmetry and cell constants. *J. Appl. Crystallogr. 26*, 795−800.
(33) Vagin, A., and Teplyakov, A. (2010) Molecular replacement with MOLREP. *Acta Crystallogr. D66*, 22−25.
(34) Murshudov, G. N., Skubák, P., Lebedev, A. A., Pannu, N. S., Steiner, R. A., Nicholls, R. A., Winn, M. D., Long, F., and Vagin, A. A. (2011) REFMAC5 for the refinement of macromolecular crystal structures. *Acta Crystallogr. D67*, 355−367.
(35) Emsley, P., and Cowtan, K. (2004) Coot: Model-building tools for molecular graphics. *Acta Crystallogr. D60*, 2126−2132.
(36) Adams, P. D., Afonine, P. V., Bunkoczi, G., Chen, V. B., Davis, I. W., et al. (2010) PHENIX: A comprehensive python-based system for macromolecular structure solution. *Acta Crystallogr. D66*, 213−221.
(37) Winn, M. D., Isupov, M. N., and Murshudov, G. N. (2001) Use of TLS parameters to model anisotropic displacements in macromolecular refinement. *Acta Crystallogr. D57*, 122−133.
(38) Davis, I. W., Leaver-Fay, A., Chen, V. B., Block, J. N., Kapral, G. J., Wang, X., Murray, L. W., Arendall, W. B., 3rd, Snoeyink, J., Richardson, J. S., and Richardson, D. C. (2007) MolProbity: All-atom contacts and structure validation for proteins and nucleic acids. *Nucleic Acids Res. 35*, W375−W383.
(39) Poirot, O., O'Toole, E., and Notredame, C. (2003) Tcoffee@igs: A web server for computing, evaluating and combining multiple sequence alignments. *Nucleic Acids Res. 31*, 3503−3506.
(40) Krissinel, E., and Henrick, K. (2004) Secondary-structure matching (SSM), a new tool for fast protein structure alignment in three dimensions. *Acta Crystallogr. D60*, 2256−2268.
(41) Schrödinger, L. (2012) The PyMOL molecular graphics system, version 1.5.0.1.
(42) Monteiro, C., Fang, X., Ahmad, I., Gomelsky, M., and Römling, U. (2011) Regulation of biofilm components in *Salmonella enterica* serovar typhimurium by lytic transglycosylases involved in cell wall turnover. *J. Bacteriol. 193*, 6443−6451.